The Adhesion GPCR ADGRL2 engages Ga13 to Enable Epidermal Differentiation

Xue Yang[1,2,10], Feng He[3,10], Douglas F. Porter[1], Krassimira Garbett[4], Robin M. Meyers[1,5], David L. Reynolds[1], Duy Lan Huong Bui[4], Audrey Hong[1], Luca Ducoli[1], Zurab Siprashvili[1], Vanessa Lopez-Pajares[1], Smarajit Mondal[1], Lisa Ko[1], Yuqing Jing[6], Shiying Tao[1], Bharti Singal[3], Richard Sando[4], Georgios Skiniotis[3,7,8]*, Paul A. Khavari[1,2,9,11]*

[1] Program in Epithelial Biology, Stanford University School of Medicine, Stanford, CA, USA.
[2] Program in Cancer Biology, Stanford University, Stanford, CA, USA.
[3] Department of Molecular and Cellular Physiology, Stanford University School of Medicine, Stanford, CA, USA
[4] Department of Pharmacology, Vanderbilt Brain Institute, Vanderbilt University, Nashville, TN 37240, USA
[5] Department of Genetics, Stanford University School of Medicine, Stanford, CA, USA
[6] Departments of Pediatrics and Genetics, Stanford University, Stanford, CA, USA
[7] Department of Structural Biology, Stanford University School of Medicine, Stanford, CA, USA
[8] Present address: Center of Excellence for Structural Cell Biology, Department of Structural Biology, St Jude Children's Research Hospital, Memphis, TN 38120, USA
[9] Veterans Affairs Palo Alto Healthcare System, Palo Alto, CA, USA.
[10] These authors contributed equally.
[11] Lead Contact.
[*] Correspondence: khavari@stanford.edu and yiorgo@stanford.edu

Abstract

Homeostasis relies on signaling networks controlled by cell membrane receptors. Although G-protein-coupled receptors (GPCRs) are the largest family of transmembrane receptors, their specific roles in the epidermis are not fully understood. Dual CRISPR-Flow and single cell Perturb-seq knockout screens of all epidermal GPCRs were thus performed, uncovering an essential requirement for adhesion GPCR ADGRL2 (latrophilin 2) in epidermal differentiation. Among potential downstream guanine nucleotide-binding G proteins, ADGRL2 selectively activated Gα13. Perturb-seq of epidermal G proteins and follow-up tissue knockouts verified that Gα13 is also required for epidermal differentiation. A cryo-electron microscopy (cryo-EM) structure in lipid nanodiscs showed that ADGRL2 engages with Gα13 at multiple interfaces, including via a novel interaction between ADGRL2 intracellular loop 3 (ICL3) and a Gα13-specific QQQ glutamine triplet sequence in its GTPase domain. In situ gene mutation of this interface sequence impaired epidermal differentiation, highlighting an essential new role for an ADGRL2-Gα13 axis in epidermal differentiation.

Introduction

The epidermis is a self-renewing surface tissue composed primarily of specialized epithelial keratinocytes that receive signals via a variety of cell surface receptors. The balance between growth and differentiation in the epidermis represents a prototype for tissue homeostasis. Dysregulation of epidermal homeostasis contributes to numerous human clinical disorders, including cancer[1], psoriasis[2] and chronic wounds[3]. GPCRs comprise the largest family of transmembrane receptors in mammals[4, 5]. Several studies have addressed the role of specific GPCRs in epidermis. For example, activating mutations in the *SMO* GPCR gene are pathogenic in basal cell carcinoma[6] and the SMO inhibitor, Vismodegib, prevents cancer progression[7]. Other examples include the Frizzled GPCR, which regulates keratinocyte proliferation[8], as well as LPAR GPCRs that enable epidermal differentiation[9]. The roles of the many other GPCRs expressed in epidermis, however, are largely uncharacterized.

Traditional pooled CRISPR screening methods are of limited utility in characterizing the actions of gene family members in epidermal homeostasis. Standard cell survival and proliferation phenotypes within bulk cell populations can fail to detect genes with essential roles in biomedically important cell transitions, such as occurs in epithelial differentiation[10]. Several CRISPR screening approaches may overcome this limitation. For example, fluorescence sorting-based pooled CRISPR screening (**CRISPR-Flow**), separates cells based on expression of marker proteins representative of specific cell states[11, 12], such as KRT10 for epidermal differentiation. Single cell Perturb RNA-sequencing (**Perturb-seq**) is another method that quantifies a subset of the transcriptome in cells undergoing a variety of genetic manipulations[13, 14]. Integrating these two methods may enable systematic evaluation of the roles of members of diverse gene families in the control of homeostatic gene expression programs.

Here we performed CRISPR-Flow and Perturb-seq knockout screens of all GPCRs expressed in epidermis. These screens validated previously reported GPCR roles while also identifying a new essential requirement for the ADGRL2 adhesion GPCR (**aGPCR**) in epidermal differentiation. ADGRL2 expression was strongly upregulated during keratinocyte differentiation. In epidermal tissue, ADGRL2 was required for induction of a key differentiation genes involved in barrier formation. Among potential downstream G proteins, ADGRL2 selectively activated Gα13 (Gα13/Gβ/Gγ). Perturb-seq screening of genes encoding Gα subunits expressed in

epidermis confirmed an essential requirement for Gα13 in epidermal differentiation. Cryo-electron microscopy (**Cryo-EM**) of nanodisc embedded ADGRL2-Gα13 complexes facilitated high-resolution structure determination. Structural analysis revealed an ADGRL2 ICL3 loop interface with a QQQ sequence on Gα13, which appears to be a unique GPCR-G protein interaction that may help explain the preferential engagement of ADGRL2 with Gα13. Mutation of the Gα13 QQQ sequence diminished ADGRL2 binding and impaired epidermal differentiation, underscoring the functional importance of this interface in newly uncovered pro-differentiation roles for the ADGRL2 GPCR and its Gα13 protein target.

Results

CRISPR-Flow and Perturb-seq of epidermal GPCRs.

Analysis of dynamic epidermal differentiation RNA-seq[15] identified 101 GPCRs expressed in epidermal keratinocytes. These span the five known GPCR sub-families (**Fig. 1a**). A CRISPR library targeting these GPCRs was next generated. sgRNAs were included to target known positive controls essential for epidermal homeostasis as well as non-targeting negative controls, encompassing 620 sgRNAs in total (**Extended Data Fig. S1a-b, Supplementary Table 1**). Quality control assessments confirmed minimal skew and full coverage of the resulting plasmid library (**Extended Data Fig. 1c**), which was designed to support both CRISPR-Flow and Perturb-seq screening assays. The CRISPR-Flow screen employed flow cytometry to isolate populations expressing high and low levels of the KRT10 epidermal differentiation marker for sgRNA enrichment/depletion analysis to nominate pro-differentiation and pro-progenitor GPCRs while the single-cell Perturb-seq screen evaluated GPCR gene knockout effects on keratinocyte progenitor and differentiation mRNA expression signatures (**Fig. 1b**). The complementary nature of these screens, one based on the expression of a single canonical early differentiation protein representing entry into the differentiation pathway and the other on the levels of a panel of keratinocyte mRNAs, was designed to catalog GPCRs with non-redundant impacts on homeostatic gene expression in epidermal keratinocytes.

Flow cytometry benchmarking for the CRISPR-Flow effort demonstrated that the KRT10-high population increased to 13.5% by day 3 of calcium-induced differentiation in vitro compared to <0.05% in day 0 progenitors (**Extended Data Fig. 1d-e**). Known positive controls required for epidermal cell differentiation, such as *IRF6, NOTCH2, PRDM1, MAF, CEBPA* and *ZNF750,* as well as the *LPAR3* GPCR, were scored by CRISPR-Flow as required for KRT10 induction. Knockout of known progenitor genes, such as *ITGB1*, *FERMT1*, *TP63*, *EGFR*, and *YAP1*, in contrast, led to increased KRT10 protein levels. These findings confirmed prior work and validated the fidelity of the screen. Among GPCRs, ADGRL2 was nominated as the strongest novel pro-differentiation GPCR (**Fig. 1c-d, Supplementary Table 2**). CRISPR-Flow screening thus validated positive controls with known impacts on homeostatic gene expression in epidermal cells while also nominating specific GPCRs as new regulators of this process.

Single-cell RNA-seq of differentiating keratinocyte populations for Perturb-seq benchmarking revealed a trajectory from progenitor-like cells to more differentiated states (**Fig. 1e**), consistent with previous studies[16]. Representative differentiation genes, such as *KRT10*, *SBSN* and *KRTDAP*, as well as undifferentiated progenitor population markers, such as *ITGB1*, *ITGA6* and *KRT14*, exhibited expected expression dynamics across pseudotime (**Fig. 1f**), supporting scRNA-seq dataset quality. As an additional quality check for CRISPR-Cas9-mediated gene knockout effectiveness, expression of targeted genes was confirmed to be significantly reduced compared to non-targeted controls (**Extended Data Fig. 1f**). Perturb-seq assigned known pro-differentiation genes, *IRF6, NOTCH2/3, PRDM1, TFAP2A*, and *GRHL3*, as well as pro-progenitor genes, *ITGB1*, *FERMT1*, *TP63*, and *YAP1* to their known roles, supporting the fidelity of the screen (**Fig. 1g-h**). As in CRISPR-Flow, Perturb-seq identified specific LPAR genes as pro-differentiation GPCRs, including *LPAR3, LPAR5 and LPAR6* (**Fig. 1g-h**), which are known to be activated by Lysophosphatidic Acid (**LPA**) and which have been previously implicated in keratinocyte differentiation[9]. ADGRL2 was again captured as a novel pro-differentiation GPCR in Perturb-seq data (**Fig. 1g-h, Extended Data Fig. 1g, Supplementary Table 3**). Correlation of the CRISPR-Flow and Perturb-seq dual screens identified ADGRL2 and LPAR3 among the top GPCR candidates promoting differentiation (**Fig. 1i**). Integration of Perturb-seq and CRISPR-Flow screens therefore nominated ADGRL2 as a novel pro-differentiation GPCR.

ADGRL2 is essential for epidermal differentiation

In keratinocyte differentiation RNA-seq datasets[15], mRNA levels of ADGRL2 were significantly upregulated during differentiation (**Extended Data Fig. 2a, red labeled**). Consistent with this, uniform manifold approximation and projection (**UMAP**) analysis performed on the Perturb-seq dataset showed that ADGRL2 mRNA levels were low in progenitors but markedly elevated in differentiated cells, concordant with *KRTDAP* differentiation gene expression and inversely correlated to the *MKI67* proliferation marker (**Fig. 2a**). Further evaluation of ADGRL2 mRNA levels showed significant upregulation during differentiation by qPCR analysis (**Fig. 2b**), along with accumulation of the self-cleaved dual protein species C-terminal fragment (**CTF**) of ADGRL2 (**Fig. 2c**). Both ADGRL2 mRNA and protein levels were therefore significantly increased during differentiation, further suggesting a possible role for ADGRL2 in this process.

In vitro, keratinocyte ADGRL2 depletion was associated with reduced differentiation mRNA levels as measured by both qPCR (**Fig. 2d, Extended Data Fig. 2b)** and RNA-seq (**Fig. 2e, Extended Data Fig. 2c, Supplementary Table 4**). Gene Ontology (**GO**) analysis of RNA-seq data showed that ADGRL2 depletion led to impaired induction of epidermal differentiation genes in patterns linked to human clinical phenotypes characterized by abnormalities in this process (**Fig. 2f**). Similarly, in 3-dimensional human skin organoid tissue regenerated from diploid human keratinocytes treated with siRNAs to ADGRL2 or scrambled control, ADGRL2 depletion led to decreases in differentiation proteins such as KRT10 and TGM1 in suprabasal epidermis, without affecting proliferation markers Ki67 (**Fig. 2g, Extended Data Fig. 2d**). To investigate whether ADGRL2 influences keratinocyte differentiation in a cell autonomous or non-cell autonomous fashion, mosaic epidermal tissue was generated by mixing HA-KRT14 labeled ADGRL2 knockdown cells with Flag-KRT14 labeled control knockdown cells at 1:1 ratios. ADGRL2-depleted cells displayed reduced KRT10 differentiation protein expression, in contrast to adjacent control cells (**Fig. 2h, Extended Data fig. 2e-f)**. These findings nominate ADGRL2 as a cell-autonomous pro-differentiation GPCR in epidermis.

ADGRL2 activates Gα13

GPCRs interact with Gα subunits of heterotrimeric G proteins to induce downstream signaling. To identify specific Gα subunits activated by ADGRL2 during keratinocyte differentiation, a TRUPATH assay[17] was employed. This approach uses the BRET2 sensor to measure the attenuation of luminescence upon downstream G protein activation[17]. To avoid interference by endogenous G proteins, a pan G protein protein-knockout (**GKO**) HEK293 cell line[18, 19] was used. Exogenously expressed ADGRL3 co-transfected with Gα13/Gβ3/Gγ9 served as a positive control and ADGRL3 co-expressed with GαoB/Gβ3/Gγ8 functioned as a negative control[20]. 12 Gα proteins are expressed across keratinocyte differentiation, as detected by RNA-seq[15]. A panel of 12 putative Gαβγ "epidermal transducerome" combinations was therefore evaluated in cells expressing either the full-length ADGRL2 or the ADGRL2 CTF, both of which correctly localized to the cell membrane (**Extended Data Fig. 3a**). Gα13 and Gα12 subunits displayed the highest basal activation levels by full-length ADGRL2 and ADGRL2-CTF (**Fig. 3a-b**). The Tethered Agonist (**TA**) peptide serves as an intrinsic ligand in aGPCRs; once exposed by proteolytic cleavage, it activates the receptor to initiate intracellular signal transduction[21]. To further dissect the role of the TA peptide in cleavage-dependent activation, therefore, two

independent systems, PAR1-ADGRL2 and EK-ADGRL2, were employed. In the PAR1-ADGRL2 system, the N-terminal extracellular portion of ADGRL2 was replaced with the N-terminal domain of protease-activated receptor PAR1, creating a TA-protected variant[22]. Thrombin treatment cleaves off the PAR1 N terminus, exposing a "scarred" TA peptide with a two amino acids deletion[22]. Localization of the PAR1-ADGRL2 hybrid protein to the cell membrane was not abolished due to these modifications (**Extended Data Fig. 3a**). Notably, despite generating a non-native "scarred" TA peptide[20, 22], the receptor still predominantly activated Gα13 upon cleavage (**Fig. 3c**). To further study this, an EK-ADGRL2 fusion was also generated. In this approach, enterokinase-mediated cleavage selectively cleaves off the SNAP tag on the N terminus of the protein and exposed a native TA peptide[20, 23]. Like the PAR1-ADGRL2 fusion, localization of the EK-ADGRL2 hybrid protein remained unchanged compared to wild-type full length ADGRL2 (**Extended Data Fig. 3a**). Upon enterokinase release of the TA peptide, the induced receptor selectively activated Gα13, reaffirming the preferential activation of Gα13 by ADGRL2 (**Fig. 3d**), and congruent with a finding reported by Pederick et al[24]. Gα13 activation by these two TA peptide cleavage mimetics of ADGRL2 are consistent with the full length ADGRL2 and ADGRL2-CTF results. As a negative control, we assessed the differential dose responses of ADGRL2-CTF and its TA peptide deletion mutant (**Δ7TA**). This mutant has no capacity to activate G proteins[25]. We also observed that the Δ7TA mutant failed to activate Gα13 in a dose-dependent fashion (**Fig. 3e**), despite similar expression and subcellular localization as ADGRL2-CTF (**Extended Data Fig. 3a-b**). Further confirmation was obtained using a Gα13 reporter SRE-RF luciferase assay, which indicated that wild-type ADGRL2-CTF displayed an enhanced ability to activate Gα13, while the Δ7TA mutant did not (**Extended Data Fig. 3c**). These data suggest that Gα13 serves as the primary Gα protein subtype activated by ADGRL2.

Gα13 is essential for epidermal tissue differentiation

To investigate if Gα13 may act in a manner consistent with a role as a downstream effector of ADGRL2 in keratinocytes, an epidermal G-protein Perturb-seq screening experiment was conducted. The Perturb-seq data confirmed that ablation of *GNA13*, the gene encoding Gα13, attenuated keratinocyte differentiation (**Extended Data Fig. 3d**). This observation was further corroborated in 2D culture, where *GNA13* depletion was associated with a significant decrease in expression of 299 differentiation-enriched genes that are also modulated by ADGRL2 (**Fig. 3f, Extended Data Fig. 3e-i, Supplementary Table 5**). These findings were then further validated

in regenerated human skin organoid tissue where, similar to *ADGRL2* loss, *GNA13* depletion reduced differentiation marker expression (**Fig. 3g, Extended Data Fig. 3j**). Gα13, like ADGRL2, is therefore required for normal induction of epidermal differentiation genes.

Cryo-EM structure of the ADGRL2-Gα13 complex in lipid nanodiscs

To examine the structural basis of Gα13 activation by ADGRL2, human ADGRL2-CTF and a miniGα13 heterotrimer were co-expressed in insect cells and reconstituted into lipid nanodiscs for Cryo-EM analysis (**Extended Data Fig. 4a-b**). The Cryo-EM map of the ADGRL2- Gα13 complex was determined at a global nominal resolution of 3.1 Å, with local refinements yielding further improved maps for the 7TM domain (2.9 Å) and G protein (2.9 Å) (**Extended Data Fig. 4c-f, Supplementary Table 6**). While previously reported aGPCR-G protein structures were determined in detergent micelles[21, 26, 27, 28, 29, 30], this ADGRL2-Gα13 complex structure provides an opportunity to examine how an aGPCR couples to G proteins in a lipid bilayer environment. Of note, two cholesterol (**CLR**)-like molecules were observed bound to the receptor in the Cryo-EM map, occupying hydrophobic cavities in between TM3 and TM4, and TM4 and TM5, respectively (**Extended Data Fig. 4g-h**). From a global perspective, the structure of the ADGRL2-Gα13 complex in lipid nanodiscs is not significantly different from the structure of the ADGRL3-Gα13 complex in detergent micelles[26] and shows a deeply buried TA peptide in the orthostatic 7TM binding site, bent TM6 and TM7 for G protein binding, and extensive interactions between ICL2 and the α5 helix (**Extended Data Fig. 4i-j**). Mutations of key ICL2 residues, such as the F943A and V942A/F943A mutants, dramatically reduced basal Gα13 activation by the ADGRL2-CTF without affecting protein localization and stability (**Extended Data Fig. 4k-m**), highlighting the broadly important role of ICL2 in the tethered agonist activation mechanism of aGPCRs[30].

ADGRL2 ICL3 in Gα13 activation

In contrast to the previously described Gα13-coupled ADGRL3 structure[26], however, the Gα13-coupled ADGRL2 structure in lipid nanodiscs revealed a distinct conformation of ICL3, which protrudes from the lipid bilayer and contacts the GTPase domain of Gα13 (**Fig. 4a, Extended Data Fig. 4n-o**). Additionally, subtle conformational differences were observed in the extracellular regions (**Extended Data Fig. 4p**). Unexpectedly, and in contrast to ADGRL3, the ICL3 of ADGRL2 appears to recognize three glutamine (**QQQ**) residues in the loop between

helix 4 and β-strand 6 of Gα13 (**Fig. 4b**), a region we observe relatively weak EM densities suggesting the dynamic character of those elements (**Extended Data Fig. 4o**). The interactions in this region likely facilitate Gα13 coupling by ordering ICL3 and promoting the outward movement of TM6, which is positioned differently than in the ADGRL3 structure (**Fig. 4b**). Indeed, 3D variability analysis, as implemented previously[31], of the global Cryo-EM map revealed that ICL3 of the receptor and this Gα13 loop flex together (**Supplementary Movie 1**). Notably, the QQQ patch of Gα13 is unique across all Gα proteins, and is not even present in its close subfamily member, Gα12, in spite of the fact that the surrounding sequences are conserved between them (**Fig. 4c**). This uniqueness suggests the potential importance for these Gα13 residues in determining the ADGRL2 coupling specificity.

To evaluate the importance of the novel ICL3-Gα13 interaction interface, a Gα13 mutant (QQQ to AAA) was generated and its basal activation by ADGRL2-CTF quantified. The AAA mutant exhibited similar expression levels to wild-type Gα13 but showed significantly reduced activity when activated by the wild-type ADGRL2-CTF (**Fig. 4d**). Moreover, the ICL2 mutant ADGRL2-CTF-F943A could partially activate wild-type Gα13 (**Fig. 4d**) but failed to appreciably activate the Gα13 AAA mutant (**Fig. 4d**), consistent with the premise that the ICL3-Gα13 interface contributes to Gα13 activation by ADGRL2. To examine the functional impact of disrupting the Gα13 QQQ interface with ADGRL2 on differentiation, the endogenous *GNA13* gene was edited in normal human keratinocytes to substitute AAA for QQQ residues in Gα13. Control editing was performed at the *GNA13* gene locus to alter codon sequences but preserve the QQQ residues to generate two isogenic keratinocyte populations genetically identical except for this sequence (**Fig. 4e**). AAA-edited keratinocytes displayed impaired differentiation gene induction while control-edited cells showed no such defects (**Fig. 4f**). These findings suggest that intactness of the newly identified ADGRL2 ICL3-Gα13 interface is required for normal epidermal differentiation.

Discussion

The results of the CRISPR-Flow and Perturb-seq GPCR screens demonstrated a degree of concordance, not only in identifying a novel role for ADGRL2 but also in detecting LPAR GPCRs with previously reported actions in epidermal differentiation. Some differences, however, were observed between the two screens in the candidate GPCRs identified, likely due to differences in their design. The CRISPR-Flow screen relied on differential sorting based on levels of a single canonical differentiation protein, KRT10, whereas the single-cell RNA-seq approach used in Perturb-seq assessed broader transcriptomic outcomes that were then placed within a single cell differentiation trajectory. In addition to ADGRL2, each knockout screen nominated specific GPCRs for future study as candidate regulators of epidermal homeostasis. Specific known and novel epidermal GPCRs, including S1PR5, GPR157, ADRA2C, GPRC5B, PTGER2, ACKR3, ADRB1, and FZD6, were top hits in CRISPR-Flow. Additional known and novel epidermal GPCRs, such as F2RL1, GPR39, BDKRB2, and GPR153 scored highly in Perturb-seq. Several GPCRs, such as S1PR5 and EDNRA, were assigned contrasting functions between the screens, underscoring the need for single GPCR-focused follow-up functional studies, as performed here for ADGRL2. Combined analysis of both screening methods identified more known and novel GPCRs than either screen alone, suggesting that integrating both methods may be useful in future efforts to identify new regulators of complex genetic programs.

The role of the third intracellular loop in GPCR signaling has been elusive, largely due to its high sequence variability and structural flexibility[32, 33, 34]. While previous structural studies of aGPCR/G protein complexes typically relied on detergent purification methods and primarily highlighted interactions involving intracellular loop 2 (ICL2) of aGPCRs[21, 26, 27, 28, 29, 30], work here utilized lipid nanodiscs[35, 36], which incorporate lipid bilayers that may help recapitulate the native environment of transmembrane proteins. This may have helped to delineate the binding interface involving both ICL2 as well as ICL3 of ADGRL2 with Gα13. The present Cryo-EM structure-defined nanodisc embedded complex reveals that the ADGRL2 ICL3 engages a unique and functionally important QQQ-containing loop sequence in the GTPase domain of Gα13, an interaction which has never been observed in previous aGPCR structural studies. The QQQ site of Gα13 is unique across all Gα proteins, and is not present in its close subfamily member, Gα12, in spite of the fact that the surrounding sequences are conserved between them. Despite the

noticeable conformational flexibility observed in the EM map, the ICL3 of ADGRL2 is positioned to bind Gα13's glutamine residues, whose mutation attenuated receptor signaling and differentiation. In agreement with a recent study showing that ICL3 modulates G protein selectivity of the β2 adrenergic receptor[37], these findings suggest a regulatory role for the ADGRL2 ICL3 in tuning receptor signaling specificity. The current data represent, to our knowledge, the first reported instance of an adhesion GPCR ICL3 engaging with a Gα protein in a structured fashion, and may thus enable future potential efforts designed to modulate signaling by ADGRL2-Gα13 as well as other aGPCRs and their corresponding Gα subunit effectors.

ADGRL1, ADGRL2, and ADGRL3 reside within the latrophilin subfamily of aGPCRs[38], which have well characterized roles in synaptic function and maintenance[39, 40]. While ADGRL1 and ADGRL3 are predominantly expressed in the brain[41, 42], ADGRL2 is expressed more widely[41, 42], suggesting it plays roles in other tissues. Actions of ADGRL2 in stratified epithelia, however, have been largely unexplored. Interestingly, both ADGRL2 mRNA and protein levels were significantly increased during differentiation. ADGRL2 knockdown impaired induction of a host of genes essential for epidermal differentiation, including a number whose mutation leads to human clinical disorders of this process. Among these genes are *TGM1, CDSN, LOR, SPINK5*, and *FLG*, each of whose mutation causes monogenic skin diseases characterized by abnormal epidermal barrier function, such as autosomal recessive congenital ichthyosis[43], peeling skin disease[44], keratoderma hereditaria mutilans[45], ichthyosis linearis circumflexa[46], and ichthyosis vulgaris[47] respectively. The ADGRL2 GPCR is therefore necessary for the induction of differentiation genes essential for formation of a healthy cutaneous barrier.

Reference

1. Ratushny V, Gober MD, Hick R, Ridky TW, Seykora JT. From keratinocyte to cancer: the pathogenesis and modeling of cutaneous squamous cell carcinoma. *J Clin Invest* **122**, 464-472 (2012).

2. Zhang X, Yin M, Zhang LJ. Keratin 6, 16 and 17-Critical Barrier Alarmin Molecules in Skin Wounds and Psoriasis. *Cells* **8**, (2019).

3. Pastar I*, et al.* Epithelialization in Wound Healing: A Comprehensive Review. *Adv Wound Care (New Rochelle)* **3**, 445-464 (2014).

4. Alhosaini K, Azhar A, Alonazi A, Al-Zoghaibi F. GPCRs: The most promiscuous druggable receptor of the mankind. *Saudi Pharm J* **29**, 539-551 (2021).

5. Weis WI, Kobilka BK. The Molecular Basis of G Protein–Coupled Receptor Activation. *Annual Review of Biochemistry* **87**, 897-919 (2018).

6. Gutzmer R, Solomon JA. Hedgehog Pathway Inhibition for the Treatment of Basal Cell Carcinoma. *Target Oncol* **14**, 253-267 (2019).

7. Sekulic A*, et al.* Efficacy and safety of vismodegib in advanced basal-cell carcinoma. *N Engl J Med* **366**, 2171-2179 (2012).

8. Ghahramani A, Donati G, Luscombe NM, Watt FM. Epidermal Wnt signalling regulates transcriptome heterogeneity and proliferative fate in neighbouring cells. *Genome Biol* **19**, 3 (2018).

9. Sumitomo A*, et al.* LPA Induces Keratinocyte Differentiation and Promotes Skin Barrier Function through the LPAR1/LPAR5-RHO-ROCK-SRF Axis. *J Invest Dermatol* **139**, 1010-1022 (2019).

10. Chen S*, et al.* Genome-wide CRISPR screen in a mouse model of tumor growth and metastasis. *Cell* **160**, 1246-1260 (2015).

11. Condon KJ*, et al.* Genome-wide CRISPR screens reveal multitiered mechanisms through which mTORC1 senses mitochondrial dysfunction. *Proc Natl Acad Sci U S A* **118**, (2021).

12. Fomicheva M, Macara IG. Genome-wide CRISPR screen identifies noncanonical NF-kappaB signaling as a regulator of density-dependent proliferation. *Elife* **9**, (2020).

13. Adamson B*, et al.* A Multiplexed Single-Cell CRISPR Screening Platform Enables Systematic Dissection of the Unfolded Protein Response. *Cell* **167**, 1867-1882 e1821 (2016).

14. Dixit A*, et al.* Perturb-Seq: Dissecting Molecular Circuits with Scalable Single-Cell RNA Profiling of Pooled Genetic Screens. *Cell* **167**, 1853-1866 e1817 (2016).

15. Kim DS*, et al.* The dynamic, combinatorial cis-regulatory lexicon of epidermal differentiation. *Nat Genet* **53**, 1564-1576 (2021).

16. Cockburn K*, et al.* Gradual differentiation uncoupled from cell cycle exit generates heterogeneity in the epidermal stem cell layer. *Nat Cell Biol* **24**, 1692-1700 (2022).

17. Olsen RHJ*, et al.* TRUPATH, an open-source biosensor platform for interrogating the GPCR transducerome. *Nat Chem Biol* **16**, 841-849 (2020).

18. Alvarez-Curto E*, et al.* Targeted Elimination of G Proteins and Arrestins Defines Their Specific Contributions to Both Intensity and Duration of G Protein-coupled Receptor Signaling. *J Biol Chem* **291**, 27147-27159 (2016).

19. Grundmann M*, et al.* Lack of beta-arrestin signaling in the absence of active G proteins. *Nature Communications* **9**, (2018).

20. Bui DLH*, et al.* The adhesion GPCRs CELSR1-3 and LPHN3 engage G proteins via distinct activation mechanisms. *Cell Rep* **42**, 112552 (2023).

21. Xiao P*, et al.* Tethered peptide activation mechanism of the adhesion GPCRs ADGRG2 and ADGRG4. *Nature* **604**, 771-778 (2022).

22. Mathiasen S*, et al.* G12/13 is activated by acute tethered agonist exposure in the adhesion GPCR ADGRL3. *Nature Chemical Biology* **16**, 1343-1350 (2020).

23. Perry-Hauser NA, VanDyck MW, Lee KH, Shi L, Javitch JA. Disentangling autoproteolytic cleavage from tethered agonist-dependent activation of the adhesion receptor ADGRL3. *J Biol Chem* **298**, 102594 (2022).

24. Pederick DT, Perry-Hauser NA, Meng H, He Z, Javitch JA, Luo L. Context-dependent requirement of G protein coupling for Latrophilin-2 in target selection of hippocampal axons. *Elife* **12**, (2023).

25. Stoveken HM, Hajduczok AG, Xu L, Tall GG. Adhesion G protein-coupled receptors are activated by exposure of a cryptic tethered agonist. *Proc Natl Acad Sci U S A* **112**, 6194-6199 (2015).

26. Barros-Alvarez X*, et al.* The tethered peptide activation mechanism of adhesion GPCRs. *Nature* **604**, 757-762 (2022).

27. Ping YQ*, et al.* Structural basis for the tethered peptide activation of adhesion GPCRs. *Nature* **604**, 763-770 (2022).

28. Qu X*, et al.* Structural basis of tethered agonism of the adhesion GPCRs ADGRD1 and ADGRF1. *Nature* **604**, 779-785 (2022).

29. Qian Y*, et al.* Structural insights into adhesion GPCR ADGRL3 activation and G(q), G(s), G(i), and G(12) coupling. *Mol Cell* **82**, 4340-4352 e4346 (2022).

30. Jones DTD, Dates AN, Rawson SD, Burruss MM, Lipper CH, Blacklow SC. Tethered agonist activated ADGRF1 structure and signalling analysis reveal basis for G protein coupling. *Nat Commun* **14**, 2490 (2023).

31. Papasergi-Scott MM*, et al.* Time-resolved cryo-EM of G-protein activation by a GPCR. *Nature* **629**, 1182-1191 (2024).

32. Probst WC, Snyder LA, Schuster DI, Brosius J, Sealfon SC. Sequence alignment of the G-protein coupled receptor superfamily. *DNA Cell Biol* **11**, 1-20 (1992).

33. Katritch V, Cherezov V, Stevens RC. Diversity and modularity of G protein-coupled receptor structures. *Trends Pharmacol Sci* **33**, 17-27 (2012).

34. Venkatakrishnan AJ, Flock T, Prado DE, Oates ME, Gough J, Madan Babu M. Structured and disordered facets of the GPCR fold. *Curr Opin Struct Biol* **27**, 129-137 (2014).

35. Denisov IG, Sligar SG. Nanodiscs for structural and functional studies of membrane proteins. *Nat Struct Mol Biol* **23**, 481-486 (2016).

36. He F*, et al.* Allosteric modulation and G-protein selectivity of the Ca(2+)-sensing receptor. *Nature* **626**, 1141-1148 (2024).

37. Sadler F, Ma N, Ritt M, Sharma Y, Vaidehi N, Sivaramakrishnan S. Autoregulation of GPCR signalling through the third intracellular loop. *Nature* **615**, 734-741 (2023).

38. Purcell RH, Hall RA. Adhesion G Protein-Coupled Receptors as Drug Targets. *Annu Rev Pharmacol Toxicol* **58**, 429-449 (2018).

39. Sando R, Sudhof TC. Latrophilin GPCR signaling mediates synapse formation. *Elife* **10**, (2021).

40. Sando R, Jiang X, Sudhof TC. Latrophilin GPCRs direct synapse specificity by coincident binding of FLRTs and teneurins. *Science* **363**, (2019).

41. Krishnan A, Nijmeijer S, de Graaf C, Schioth HB. Classification, Nomenclature, and Structural Aspects of Adhesion GPCRs. *Handb Exp Pharmacol* **234**, 15-41 (2016).

42. Regan SL, Williams MT, Vorhees CV. Latrophilin-3 disruption: Effects on brain and behavior. *Neurosci Biobehav Rev* **127**, 619-629 (2021).

43. Herman ML*, et al.* Transglutaminase-1 gene mutations in autosomal recessive congenital ichthyosis: summary of mutations (including 23 novel) and modeling of TGase-1. *Hum Mutat* **30**, 537-547 (2009).

44. van der Velden J, van Geel M, Engelhart JJ, Jonkman MF, Steijlen PM. Mutations in the CDSN gene cause peeling skin disease and hypotrichosis simplex of the scalp. *J Dermatol* **47**, 3-7 (2020).

45. Pohler E*, et al.* Novel autosomal dominant mutation in loricrin presenting as prominent ichthyosis. *Br J Dermatol* **173**, 1291-1294 (2015).

46. Guerra L*, et al.* Ichthyosis Linearis Circumflexa as the Only Clinical Manifestation of Netherton Syndrome. *Acta Derm Venereol* **95**, 720-724 (2015).

47. Thyssen JP, Godoy-Gijon E, Elias PM. Ichthyosis vulgaris: the filaggrin mutation disease. *Br J Dermatol* **168**, 1155-1166 (2013).

Figure Legends

Fig. 1. CRISPR-Flow and Perturb-seq screens in differentiating normal human keratinocytes. a, Pie chart of the 101 epidermal GPCRs and their classes. **b**, Schematic of experimental workflow for CRISPR screens. **c**, Scatterplot mapping guide enrichment (beta score) in low vs. high KRT10 cells from CRISPR-Flow screening. **d**, Bar graphs quantifying mean beta scores from top CRISPR-Flow identified candidates (red=GPCRs, black=controls). **e**, Principal Component Analysis (PCA) plot representing variance in gene expression between progenitor and differentiated epidermal states at day 3. **f**, Pseudotime trajectory analysis of progenitor markers ITGB1/KRT14/ITGA6 and differentiation markers KRTDAP/SBSN/KRT10 at day 3. **g**, Perturb-seq GPCR and positive control target effects plotted as pseudotime differences from non-target guides (Z score) *vs* Mann-Whitney p values for the comparison to cells with other guides. **h**, Enrichment of knock-out cells along the pseudotime trajectory (Mann-Whitney log10 P) compared to cells with safe target guides. A positive enrichment in low pseudotime cells indicates nominates a gene as necessary for differentiation. **i**, Correlation analysis of CRISPR-Flow beta scores plotted against Perturb-seq pseudotime measurements for each CRISPR target. ADGRL2 is highlighted in red. For all analyses *=p<0.05, **=p<0.01, ***=p<0.001.

Fig. 2. Requirement for ADGRL2 in epidermal differentiation. a, UMAP analysis depicting ADGRL2 expression in progenitor and differentiated states in scRNA-seq data. **b**, ADGRL2 mRNA levels across keratinocyte differentiation in vitro. **c**, ADGRL2 protein levels (C-terminal fragment dual bands) across differentiation. **d**, mRNA expression by qPCR of differentiation markers and progenitor markers with control versus ADGRL2 knockdown (L2 si1 and L2 si2) from four independent human skin donors evaluated. **e**, RNA-Seq analysis of ADGRL2 knockdown keratinocytes sourced from three unrelated skin donors, showing all genes with log2 fold change >0.2 or <-0.2, red/blue genes are the ones upregulated/downregulated during differentiation, white genes are unchanged ones. **f**, Gene Ontology analysis of all significantly altered mRNAs (FDR<0.05) following ADGRL2 knockdown based on the RNA-seq data. **g**, Immunostaining of KRT10, TGM1 and Ki67 in regenerated human skin organoid tissue with ADGRL2 depletion versus control. **h**, Immunostaining of KRT10 in mosaic skin organoids. In **b**

and **c**, one-way ANOVA with Dunnett's test against day 0 cells, n = 3. In **d**, one-way ANOVA with Dunnett's test against control cells for each gene, n = 4.

Fig. 3. ADGRL2 activates Gα13. (**a, b**) Domain structures, the net BRET2 signals and summarized BRET2 heatmap from full-length ADGRL2 and ADGRL2-CTF. (**c, d**) Domain structures with drug treatment conditions, the induced BRET2 signals and summarized BRET2 heatmap from PAR1-ADGRL2 and EK-ADGRL2. **e**, Dose-dependent BRET2 signaling profiles of ADGRL2-CTF and ADGRL2 TA peptide deficient mutants (Δ7TA) on Gα13. **f**, Gene Ontology analysis of 299 significant altered mRNAs (FDR<0.1) shared between *GNA13* and *ADGRL2* knockdown RNA-seq datasets. **g**, Immunostaining for KRT10 and TGM1 in human skin organoid tissues with Gα13 depletion. In **e**, two-way ANOVA with Dunnett's test against each dosage of wild-type ADGRL2-CTF condition, n=3.

Fig. 4. Structure of the ADGRL2-Gα13 complex. a, Cryo-EM map of the ADGRL2-Gα13 complex in a lipid nanodisc. The ADGRL2 ICL3 protrudes from the lipid bilayer and is highlighted with a dashed blue box. **b**, Comparison of the Gα13-coupled ADGRL2 and ADGRL3 structures showing conformational differences in ICL3 and TM6 (highlighted by arrows). In contrast to that in the ADGRL3 structure, the ICL3 of ADGRL2 is more ordered and shifts towards Gα13 to interact with a loop region containing three glutamine (QQQ) residues (shown as sticks). **c**, Sequence alignment of different Gα subtypes (including Gαs-short, Gαi, Gαq, Gα12 and Gα13) focusing on the distinct feature of three glutamine residues (QQQ) within the loop connecting helix 4 and β-strand 6 in Gα13. **d**, Effects of alanine substitution of the Gα13 QQQ triplet on the basal activity of ADGRL2-CTF WT and the ICL2 mutant (F943A). **e**, Gene editing tracks and efficiency of AAA substitution for QQQ sequences at the endogenous *GNA13* gene in bulk primary human keratinocyte populations. **f**, mRNA expression of early differentiation markers with GNA13 QQQ and AAA edited cells evaluated by qPCR. In **d**, two-way ANOVA with Dunnett's test against each dosage of wild-type ADGRL2-CTF + wild-type Gα13 condition, n=3 or 4. In **f**, One-way ANOVA with Dunnett's test against control Gα13 QQQ cells, n = 3.

Figure 1 Using CRISPR-Flow and Perturb-Seq to identify a functional role for the GPCRs in epidermal hemomeostasis.

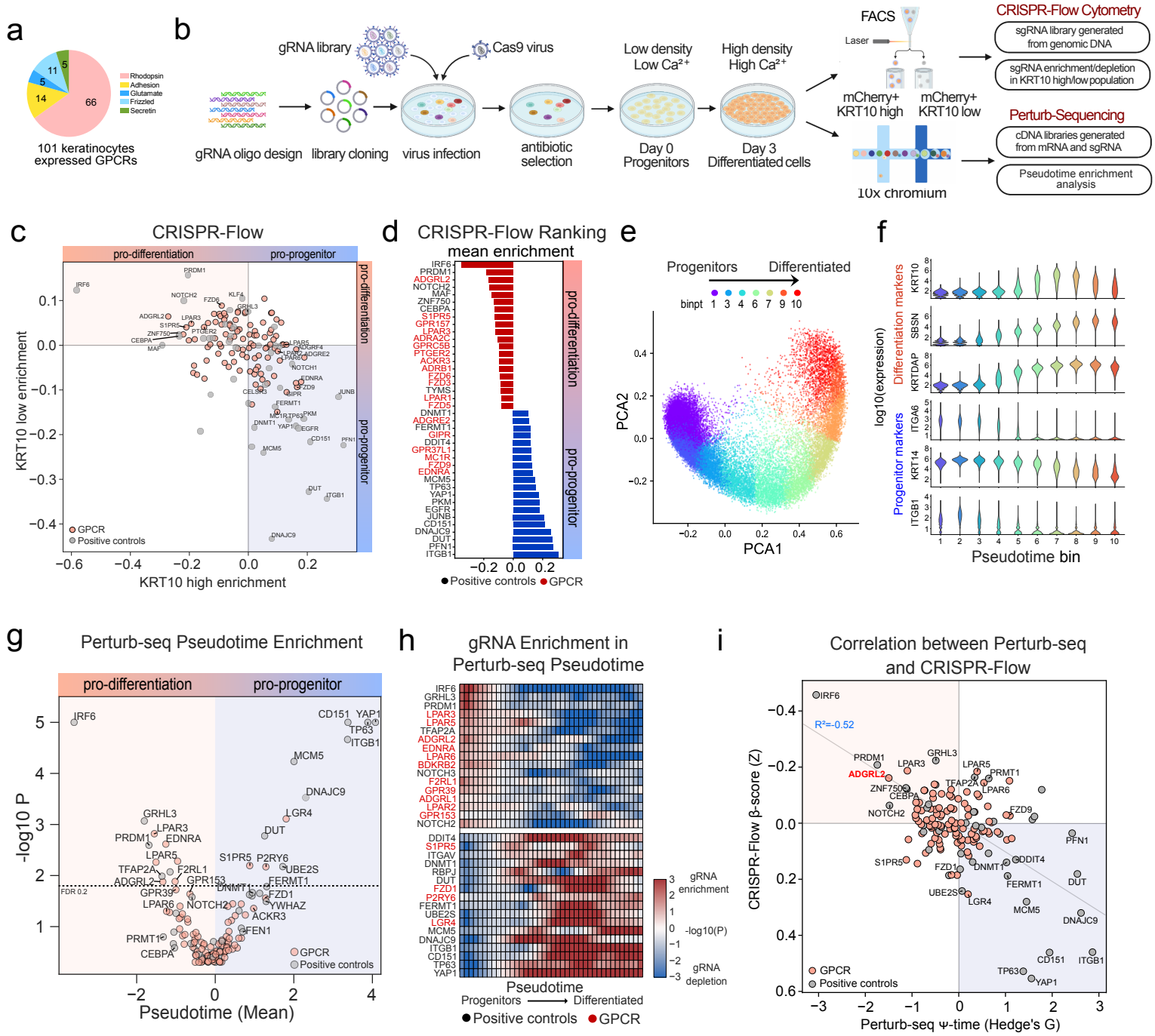

Figure 2 ADGRL2 is essential for normal epidermal differentiation

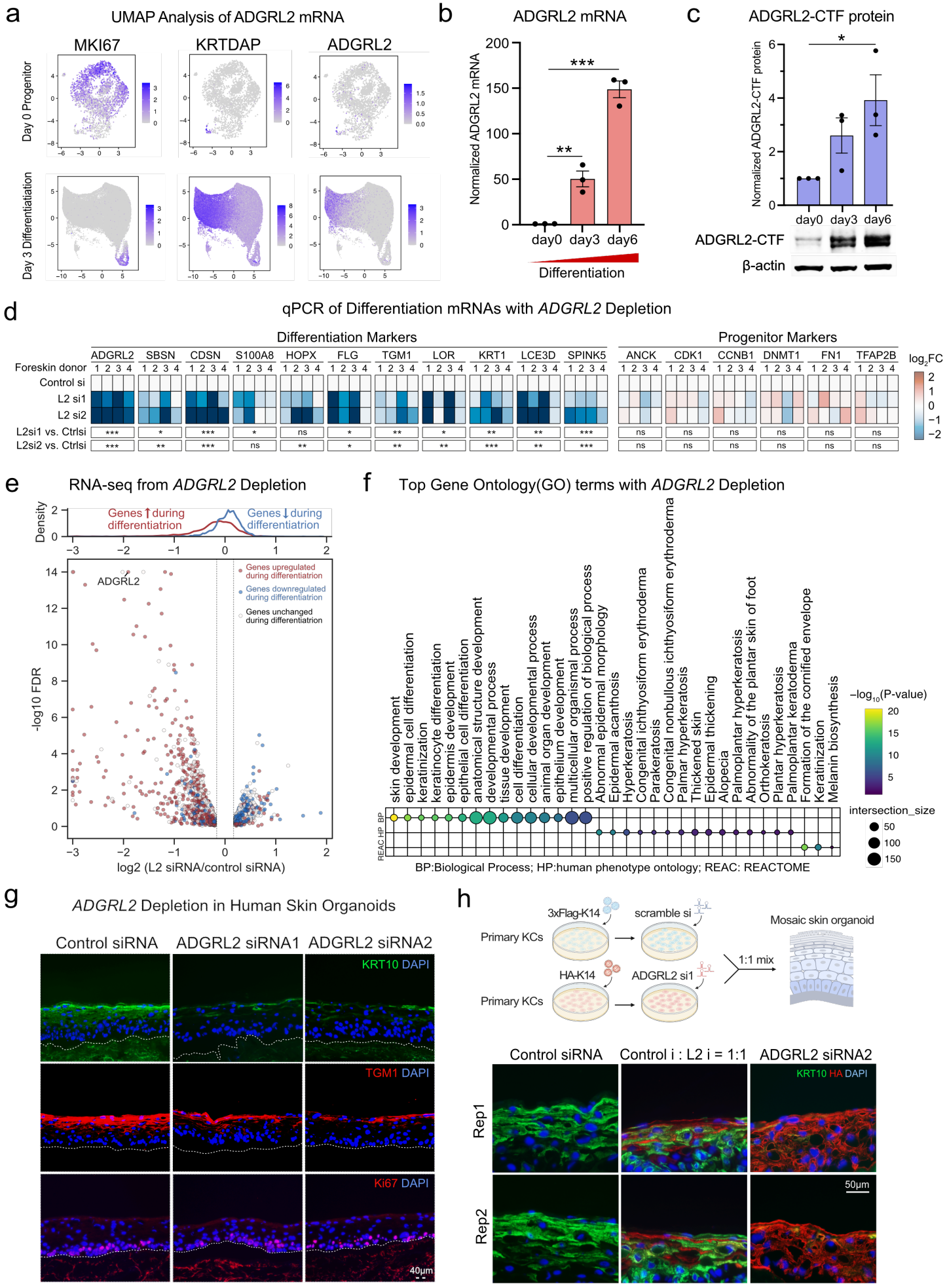

Figure 3 ADGRL2 activates Gα13 to guide epidermal differentiation

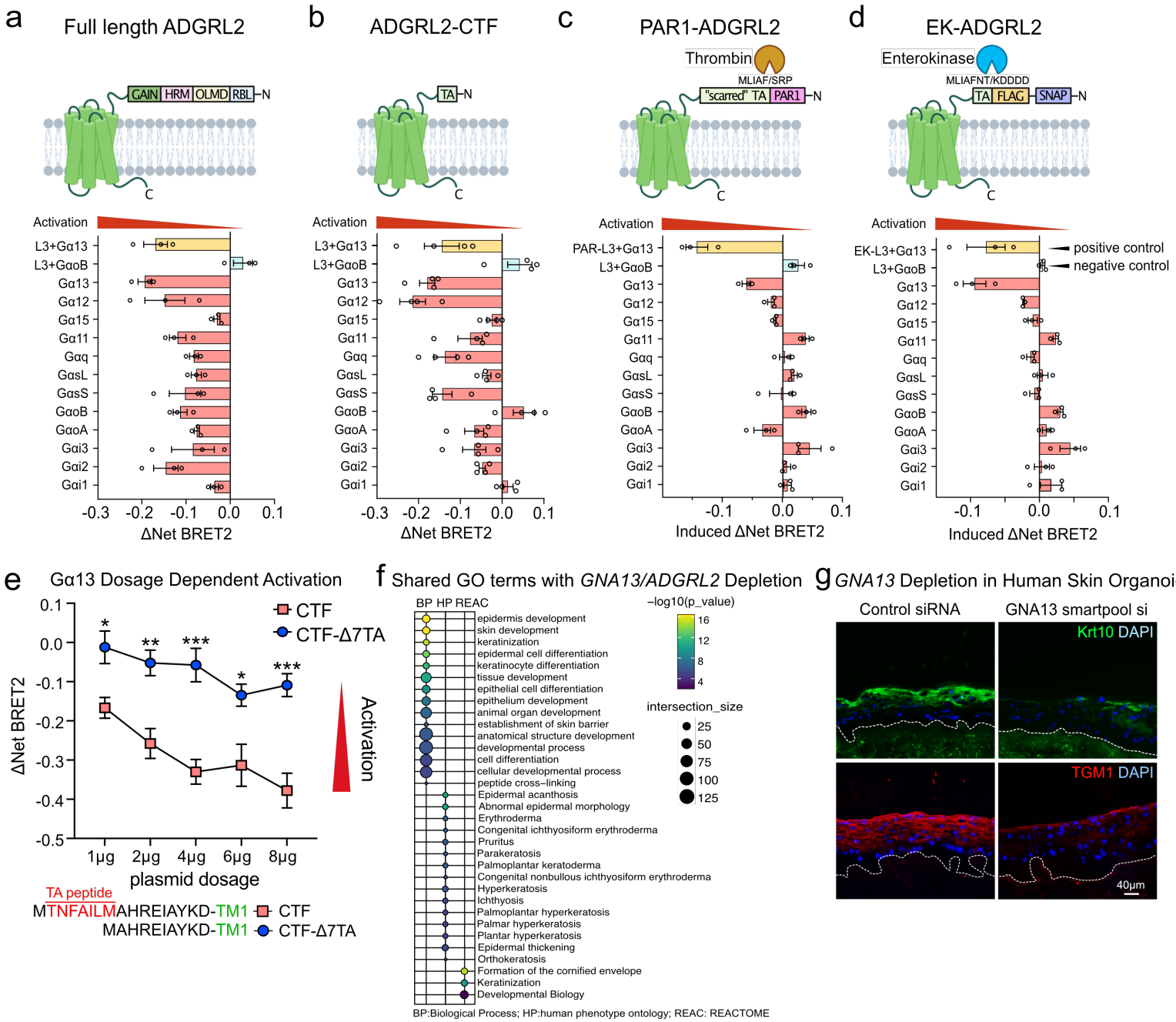

Figure 4 ADGRL2 ICL3 in Gα13 activation

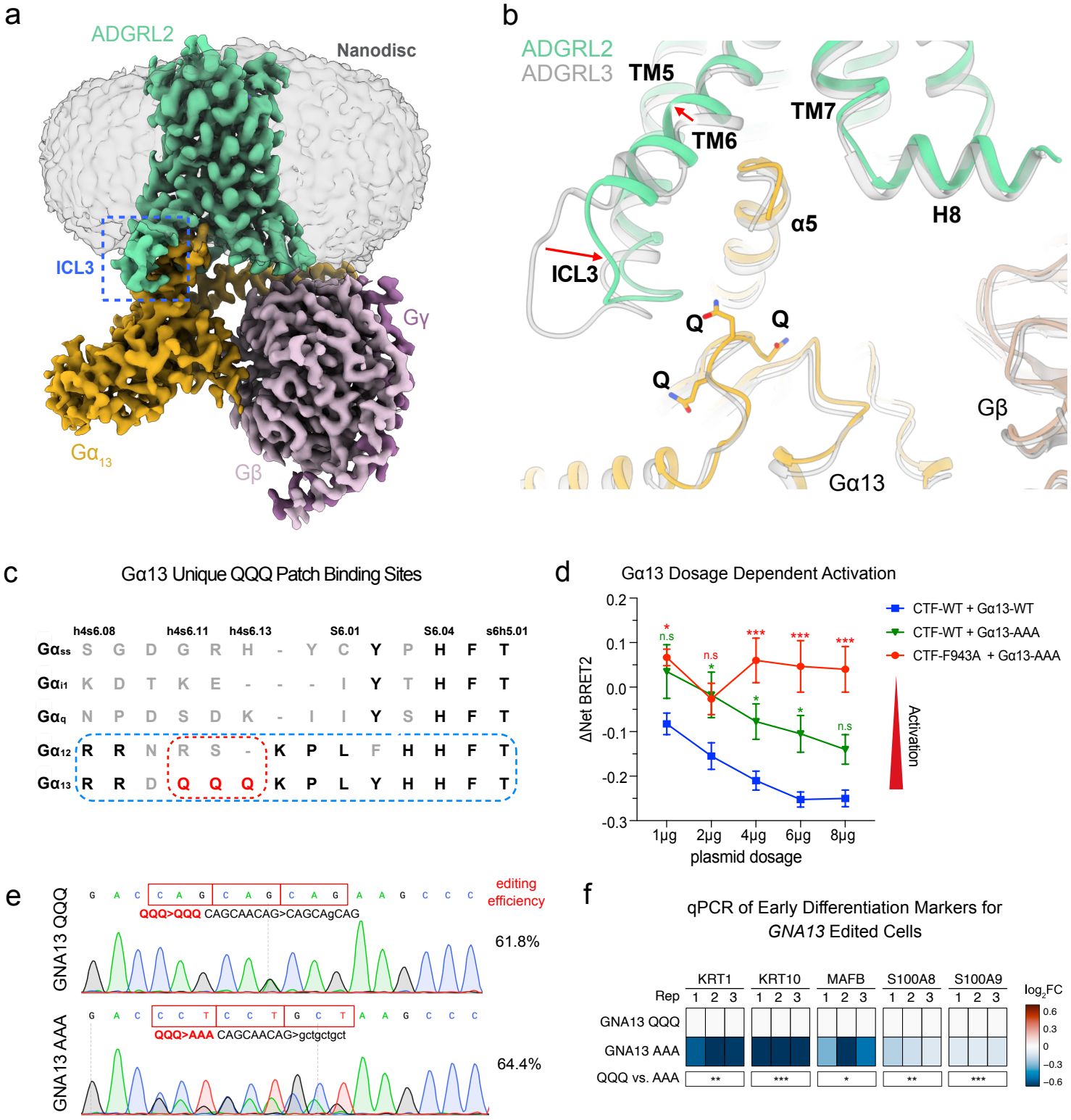

Figure 1S

a

Categories	Gene numbers	gRNAs
GPCR	101	404
Keratinocytes control genes	22	88
Progenitor control genes	22	88
Non-target gRNAs	NA	40
Total	145	620

b

Keratinocyte differentiation associated genes

IRF6	GRHL3	MAF	MCM5	PKM	DUT
ZNF750	POU2F3	MAFB	ITGB1	PFN1	FEN1
KLF4	JUNB	VDR	FERMT1	DNMT1	ARPC1B
CEBPA	PRDM1	TP63	CD151	YWHAZ	DDIT4
EHF	OVOL1	YAP1	EGFR	S100A8	
NOTCH1	TFAP2A	PRMT1	DNAJC9	MGST1	
NOTCH2	HOPX	CALML3	UBE2S	ITGAV	
RBPJ	MPZL3	NOTCH3	SFN	TYMS	

c

gRNA reads distribution
90%/10%=2.03

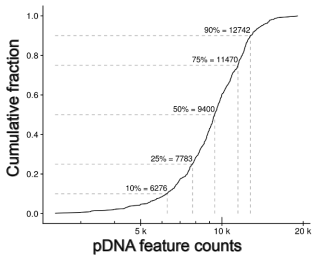

d

Overall gating strategy

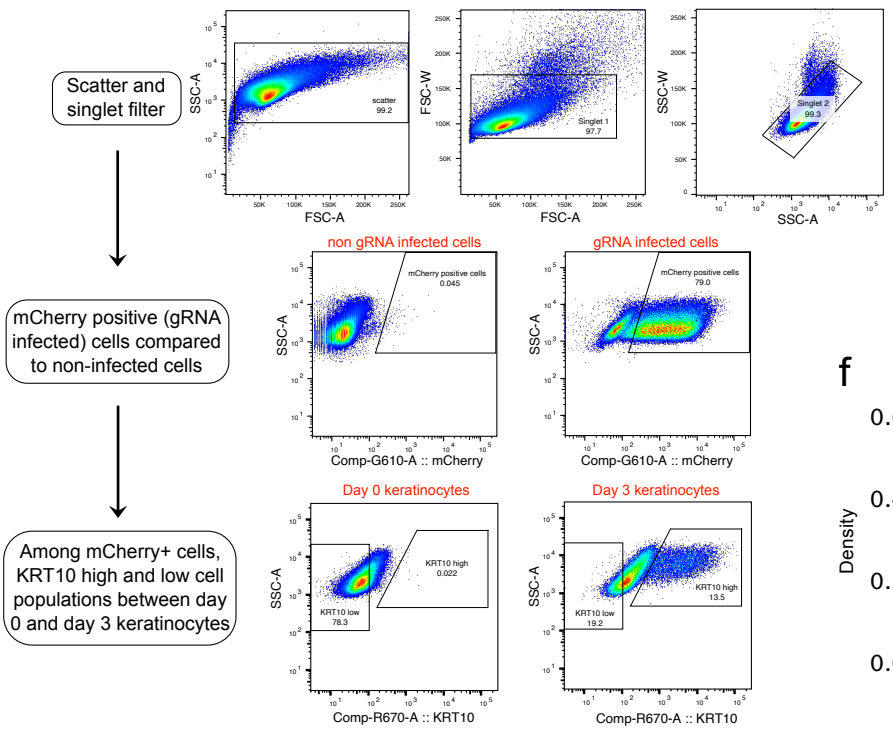

e

KRT10 enrichment

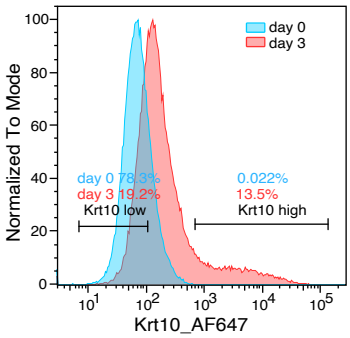

f

target mRNA level in perturb-seq

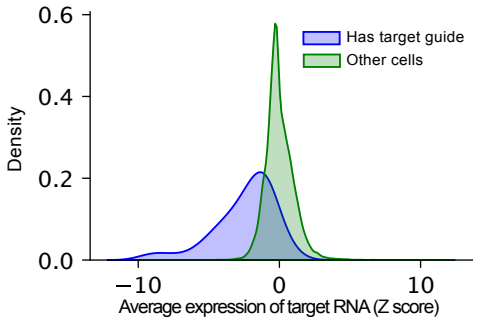

g

Perturb-seq heatmap

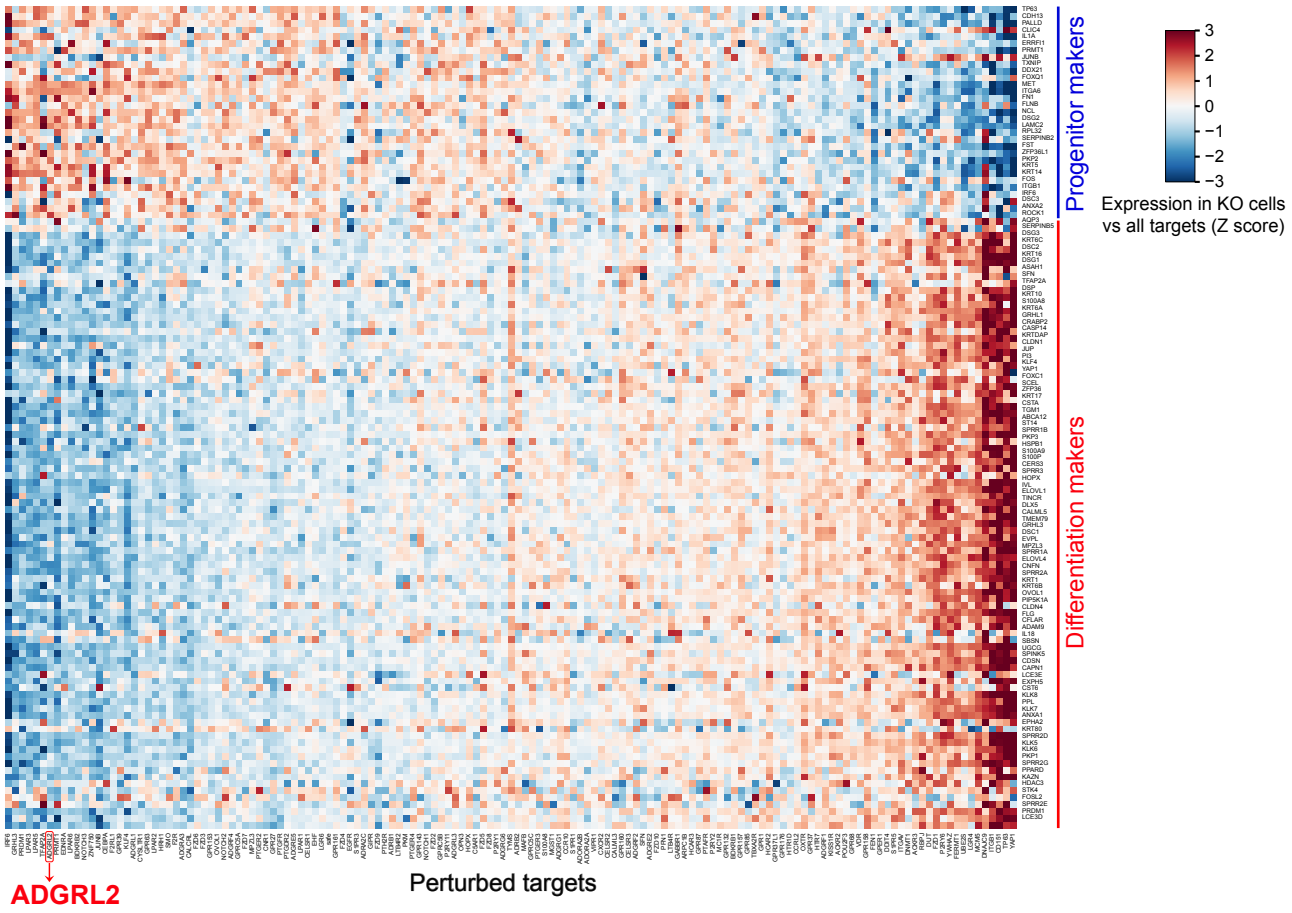

Figure 2S

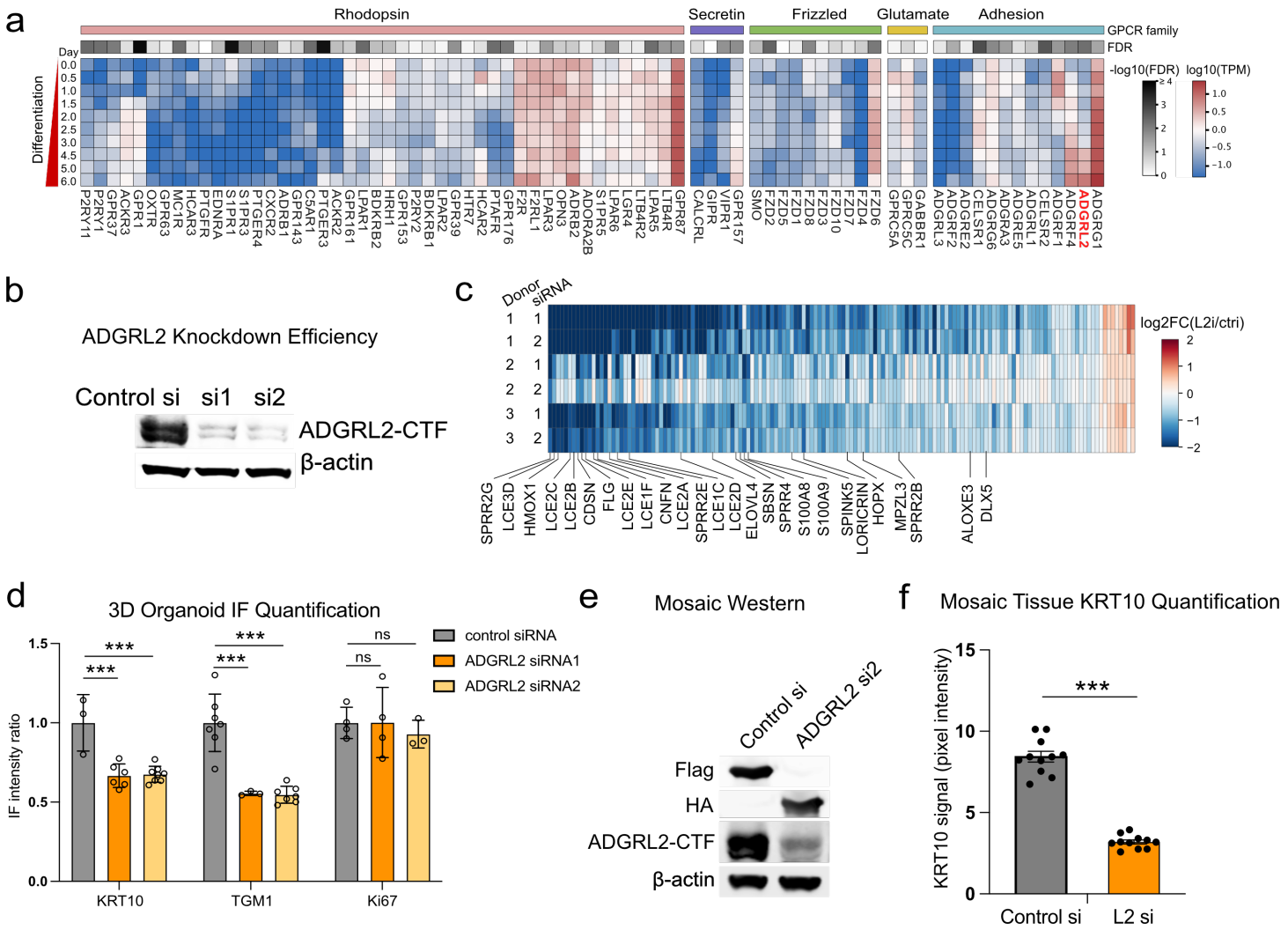
a
Rhodopsin
Secretin
Frizzled
Glutamate
Adhesion
GPCR family
FDR
Day
Differentiation
-log10(FDR)
log10(TPM)
b
ADGRL2 Knockdown Efficiency
Control si
si1
si2
ADGRL2-CTF
β-actin
c
Donor
siRNA
log2FC(L2i/ctri)
d
3D Organoid IF Quantification
control siRNA
ADGRL2 siRNA1
ADGRL2 siRNA2
IF intensity ratio
KRT10
TGM1
Ki67
e
Mosaic Western
Control si
ADGRL2 si2
Flag
HA
ADGRL2-CTF
β-actin
f
Mosaic Tissue KRT10 Quantification
KRT10 signal (pixel intensity)
Control si
L2 si

Figure 3S

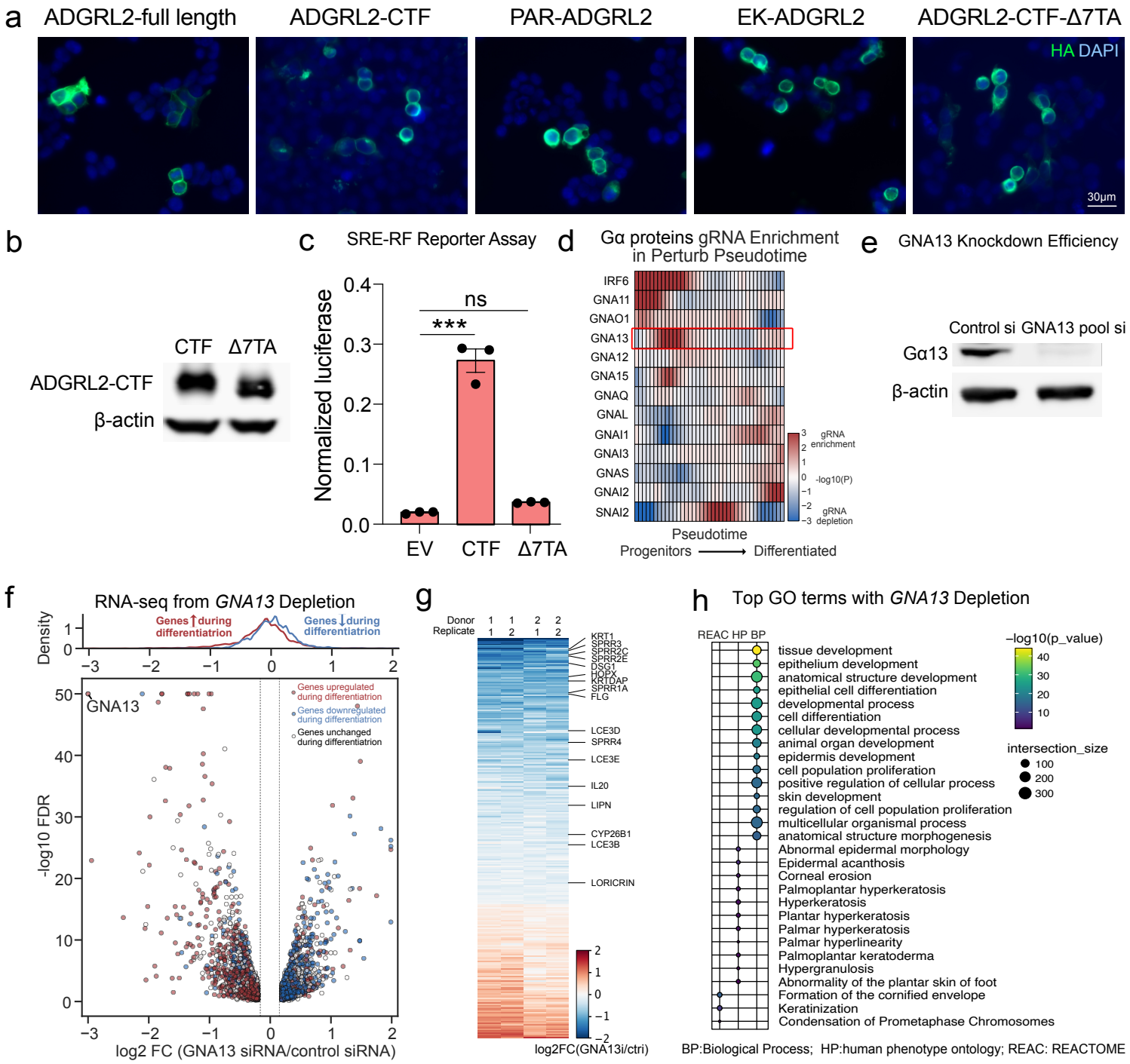
a
ADGRL2-full length
ADGRL2-CTF
PAR-ADGRL2
EK-ADGRL2
ADGRL2-CTF-Δ7TA
HA DAPI
30μm
b
CTF
Δ7TA
ADGRL2-CTF
β-actin
c
SRE-RF Reporter Assay
Normalized luciferase
ns
***
EV
CTF
Δ7TA
d
Gα proteins gRNA Enrichment in Perturb Pseudotime
IRF6
GNA11
GNAO1
GNA13
GNA12
GNA15
GNAQ
GNAL
GNAI1
GNAI3
GNAS
GNAI2
SNAI2
gRNA enrichment
-log10(P)
gRNA depletion
Pseudotime
Progenitors
Differentiated
e
GNA13 Knockdown Efficiency
Control si
GNA13 pool si
Gα13
β-actin
f
RNA-seq from GNA13 Depletion
Density
Genes ↑ during differentiatrion
Genes ↓ during differentiatrion
GNA13
Genes upregulated during differentiatrion
Genes downregulated during differentiatrion
Genes unchanged during differentiatrion
-log10 FDR
log2 FC (GNA13 siRNA/control siRNA)
g
Donor
Replicate
KRT1
SPRR3
SPRR2C
SPRR2E
DSG1
HOPX
KRTDAP
SPRR1A
FLG
LCE3D
SPRR4
LCE3E
IL20
LIPN
CYP26B1
LCE3B
LORICRIN
log2FC(GNA13i/ctri)
h
Top GO terms with GNA13 Depletion
REAC HP BP
tissue development
epithelium development
anatomical structure development
epithelial cell differentiation
developmental process
cell differentiation
cellular developmental process
animal organ development
epidermis development
cell population proliferation
positive regulation of cellular process
skin development
regulation of cell population proliferation
multicellular organismal process
anatomical structure morphogenesis
Abnormal epidermal morphology
Epidermal acanthosis
Corneal erosion
Palmoplantar hyperkeratosis
Hyperkeratosis
Plantar hyperkeratosis
Palmar hyperkeratosis
Palmar hyperlinearity
Palmoplantar keratoderma
Hypergranulosis
Abnormality of the plantar skin of foot
Formation of the cornified envelope
Keratinization
Condensation of Prometaphase Chromosomes
−log10(p_value)
intersection_size
BP:Biological Process; HP:human phenotype ontology; REAC: REACTOME
i
ADGRL2 and GNA13 Depletion RNA-seq Overlap Hits
Genes upregulated during differentiatrion
Genes downregulated during differentiatrion
Genes unchanged during differentiatrion
R²=0.16
log2FC(GNA13 si/control si)
log2FC(L2 si/control si)
j
3D Organoid IF Quantification
**
***
control siRNA
GNA13 smartpool siRNA
KRT10
TGM1

Figure 4S

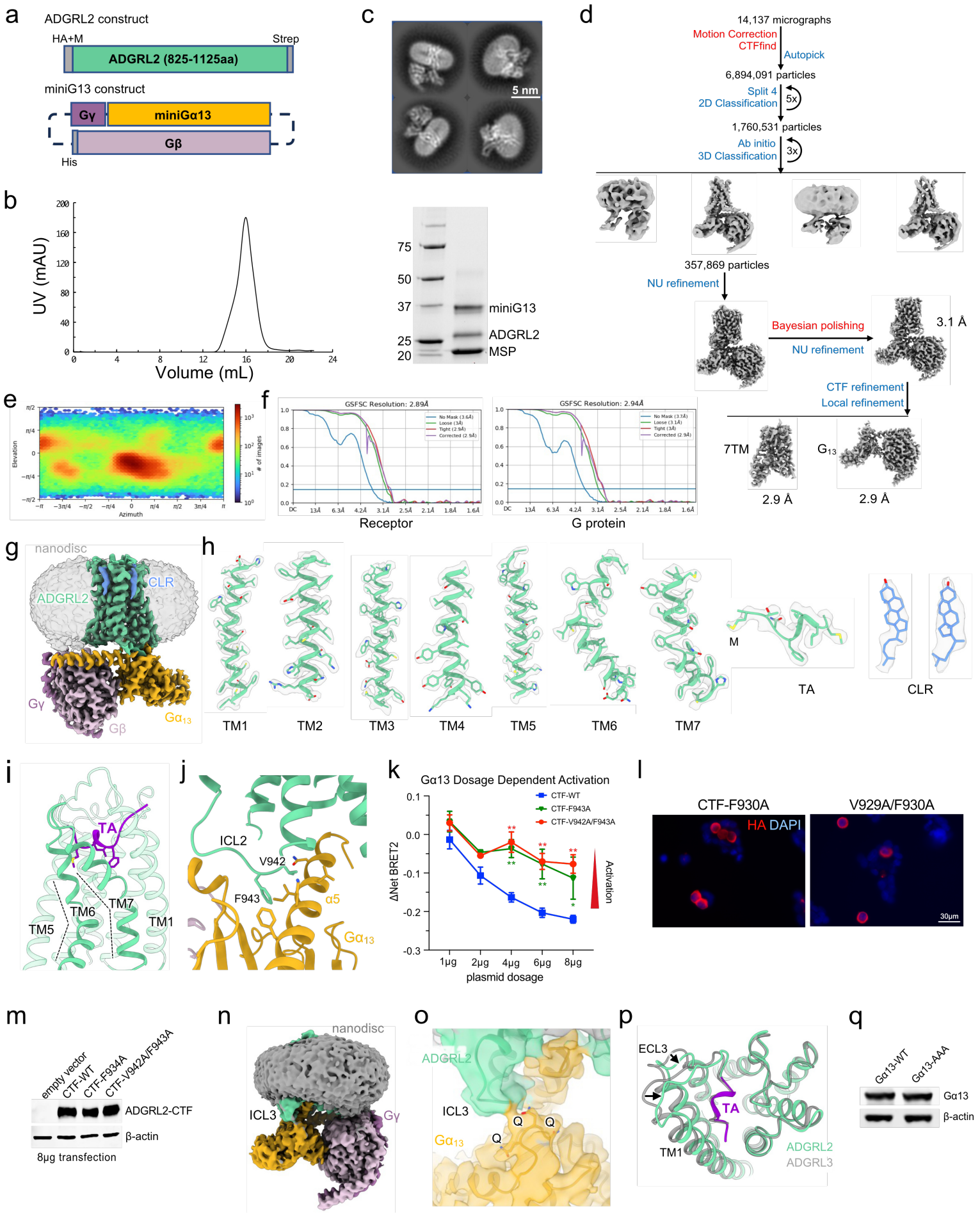
a
ADGRL2 construct
HA+M
Strep
ADGRL2 (825-1125aa)
miniG13 construct
Gγ
miniGα13
Gβ
His
b
UV (mAU)
Volume (mL)
c
5 nm
75
50
37
25
20
miniG13
ADGRL2
MSP
d
14,137 micrographs
Motion Correction
CTFfind
Autopick
6,894,091 particles
Split 4
2D Classification
5x
1,760,531 particles
Ab initio
3D Classification
3x
357,869 particles
NU refinement
Bayesian polishing
NU refinement
3.1 Å
CTF refinement
Local refinement
7TM
Gi
2.9 Å
2.9 Å
e
Elevation
Azimuth
# of images
f
GSFSC Resolution: 2.89Å
GSFSC Resolution: 2.94Å
Receptor
G protein
g
nanodisc
ADGRL2
CLR
Gγ
Gβ
Gα13
h
TM1
TM2
TM3
TM4
TM5
TM6
TM7
M
TA
CLR
i
TA
TM5
TM6
TM7
TM1
j
ICL2
V942
F943
α5
Gα13
k
Gα13 Dosage Dependent Activation
CTF-WT
CTF-F943A
CTF-V942A/F943A
ΔNet BRET2
Activation
1μg
2μg
4μg
6μg
8μg
plasmid dosage
l
CTF-F930A
V929A/F930A
HA DAPI
30μm
m
empty vector
CTF-WT
CTF-F934A
CTF-V942A/F943A
ADGRL2-CTF
β-actin
8μg transfection
n
nanodisc
ICL3
Gγ
o
ADGRL2
ICL3
Gα13
Q
p
ECL3
TA
TM1
ADGRL2
ADGRL3
q
Gα13-WT
Gα13-AAA
Gα13
β-actin